

Constraining Proper Motion of Strongly Lensed Eccentric Binary Mergers using Doppler Triangulation

JOHAN SAMSING,¹ LORENZ ZWICK,¹ PANKAJ SAINI,¹ KAI HENDRIKS,¹ RICO K. L. LO,¹ LUKA VUJEVA,¹ GEORGI D. RADEV,² AND YAN YU²

¹*Niels Bohr International Academy, The Niels Bohr Institute, Blegdamsvej 17, DK-2100, Copenhagen, Denmark*

²*The Niels Bohr Institute, Blegdamsvej 17, DK-2100, Copenhagen, Denmark*

(Dated: January 23, 2025)

ABSTRACT

Strong lensing of gravitational wave (GW) sources allows the observer to see the GW source from different lines-of-sight (LOS) through the corresponding images, which provides a way for constraining the relative proper motion of the GW source. This is possible as the GW signals received from each image will have slightly different projected velocity components, from which one can ‘Doppler-Triangulate’ for the GW source velocity vector. The difference in projected velocity between the different images can be observationally inferred through pairwise GW phase measurements that accumulate over the time-of-observation. In this paper we study lensed eccentric GW sources and explore how the observable GW phase shift between images evolve as a function of time, eccentricity, lens- and binary parameters. Next generation GW observatories, including the Einstein Telescope and Cosmic Explorer, will see \sim hundreds/year of lensed GW sources, where a significant fraction of these are expected to be eccentric. We discuss the expected unique observables for such eccentric lensed GW sources, and the relation to their observable relative linear motion, which otherwise is exceedingly difficult to constrain in general.

1. INTRODUCTION

Observations of strong gravitationally lensed gravitational wave (GW) sources, provide not only information about the lens, but also unique information about the GW source itself. One such unique measure relates to the transverse proper motion of the GW source relative to the lens and the observer (e.g. Itoh et al. 2009; Savastano et al. 2024; Samsing et al. 2024b), which can be constrained when two or more images are observed. Recently in Samsing et al. (2024b), this was shown to be possible using ground-based detectors, such as Einstein Telescope (ET) and Cosmic Explorer (CE), that are expected to observe \sim hundreds of strongly lensed GW source per year (e.g. Xu et al. 2022; Smith et al. 2023). Constraining the proper motion of GW sources is exceedingly hard for GW mergers in general due to the absence of characteristic length- or mass scales associated with individual events, as well as due to the difficulty in disentangling proper motion from the Hubble flow. Observations of strongly lensed GW sources therefore have the potential to provide key insights into aspects related to GW sources, their host environment, dynamics and possible underlying formation mechanisms, which otherwise are not generally accessible through standard single GW events.

The relative transverse velocity of GW sources can be measured in strongly lensed events, as each lens image es-

entially makes it possible for the observer to see the GW source from different directional lines-of-sight (LOS) (Samsing et al. 2024b). As the velocity vector of the GW source projects differently onto the different LOS, the corresponding GW images will have different Doppler factors, which implies that the received GW signals will appear red- or blue-shifted relative to each other. In a flat static universe, the projected difference in radial velocity as observed between two images, is by geometry (see Fig. 1) given by $\Delta v \approx 2\theta v$, where v is the relative transverse velocity of the GW source, and 2θ is the angular separation between the two lensed images. This velocity difference gives rise to the relative Doppler factor, $\sim \Delta v/c$, that can be linked to a displacement in angular phase of the received GW signals; a measurement of GW phase shift between images can therefore be used to constrain the relative transverse motion of the GW source. When three or more images are seen, one can triangulate for a better estimate of the direction of the GW source velocity vector, explaining why we refer to this method as *Doppler-Triangulation*. Variations of this method have been discussed a few places, both in terms of electromagnetic signals (Kayser et al. 1986; Chitre & Saslaw 1989; Birkinshaw 1989; Wucknitz & Sperhake 2004), as well as for GW systems (e.g. Itoh et al. 2009; D’Orazio & Loeb 2020; Gondán & Kocsis 2022; Yang et al. 2024; Savastano et al. 2024) with implications for deci-hertz detectors such as DECIGO/TianQin/Taiji (Kawamura et al. 2011; Luo

et al. 2016; Hu & Wu 2017; Liu et al. 2020), and then recently with applications for ground-based detectors (Samsing et al. 2024b).

Past studies and results have all been based on lensed circular GW sources. However, recent theoretical advances in black hole dynamics hint that a significant fraction of GW sources likely evolve into the observable bands with significant eccentricity (e.g. Gültekin et al. 2006; Samsing et al. 2014; Samsing & Ramirez-Ruiz 2017; Samsing & Ilan 2018; Samsing et al. 2018b; Samsing 2018; Samsing et al. 2018a; Samsing & D’Orazio 2018; Rodriguez et al. 2018; Liu et al. 2019; Zevin et al. 2019; Samsing et al. 2019, 2020; Zevin et al. 2021; Samsing et al. 2022; Fabj & Samsing 2024). As demonstrated in e.g. Samsing et al. (2024a); Hendriks et al. (2024a,b), the GW phase shift for accelerated eccentric GW sources, i.e. for sources with a $|dv/dt| > 0$, generally evolves very differently compared to circular GW sources. It is therefore of great importance to understand how the GW phase shift between images of strongly lensed eccentric GW events evolve in our considered case of moving sources, and how the observables differ from the circular limit.

With this motivation, we here study for the first time the relationship between the relative proper motion of strongly lensed eccentric GW sources and the resultant observable GW phase shift between the images. Assuming a constant relative transverse motion between lens, GW source, and observer, we especially explore the evolution of the GW phase shift as a function of time, GW frequency, and eccentricity. It is not yet understood if GW sources with different formation pathways, e.g. dynamical formation relative to isolated binary formation, can be disentangled through their velocity flow linked to their host system. However, our promising study serves as an excellent starting point for looking into this further, as well as to prepare for a future of learning from both eccentric- and circular strongly lensed GW sources.

The paper is organized as follows. In Sec. 2 we describe the basics of inferring relative transverse motion of strongly lensed GW sources from GW phase shift measurements between images. In Sec. 3 we provide our analytical solution applied to eccentric GW sources, after which we conclude our study in Sec. 4.

2. CONSTRAINING PROPER MOTION OF GRAVITATIONAL WAVE SOURCES

2.1. Theory and Observables

We consider a setup composed of three planes; the *Observer plane*, the *Lens plane*, and the *Source plane*, as shown in Fig. 1. In an expanding universe, the relative velocities translate non-trivially between these planes, as time and length scale with the expansion, or redshift, z . Following Kayser et al. (1986); Itoh et al. (2009); Samsing et al. (2024b), this implies that for the general case where the observer, lens and source

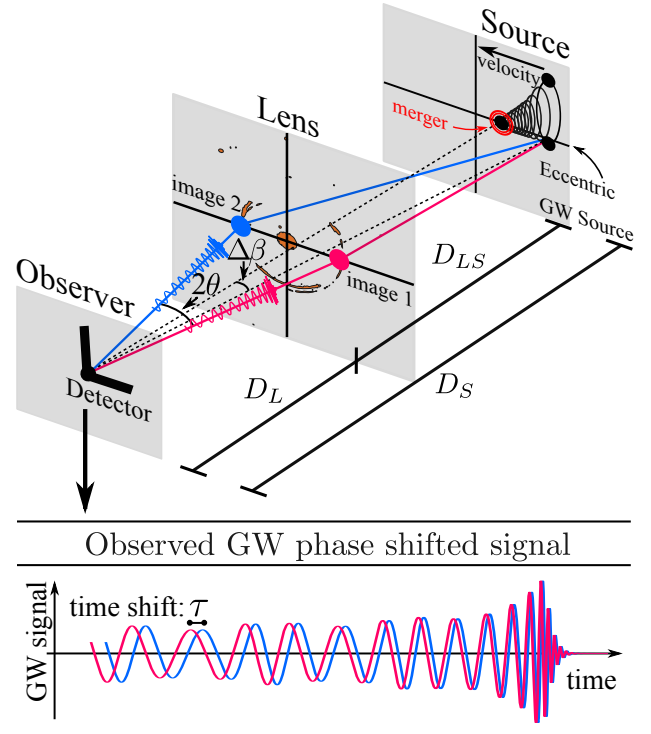


Figure 1. Illustration of a Strongly Lensed Eccentric Gravitational Wave Source. The *Top Panel* shows the Observer-Lens-Source setup, with the detector in the *Observer-plane*, the gravitational lens in the *Lens-plane*, and the lensed eccentric GW source in the *Source-plane*. The eccentric GW source moves here in the source plane over a duration time t , that corresponds to a change in angular position $\Delta\beta$ and time-delay, τ . The observer sees the lensed GW source through the two images; *image 1* and *image 2*, that provide two different LOS towards the source, implying that the received signals generally will have slightly different Doppler factors. For GW sources, this manifests as a GW phase shift, as illustrated in the *Bottom Panel*, that can be observed and then related to the linear motion of the GW source relative to the lens and observer. If three or more images are observed, one can make a *Doppler-Triangulation* for better constraining the magnitude and direction of the velocity vector.

each move in their own respective frames with transverse velocity v_O , v_L , and v_S , respectively, that one can define an effective velocity of the GW source in its source plane as,

$$v' = v_S - \frac{1+z_S}{1+z_L} \frac{D_S}{D_L} v_L + \frac{1+z_S}{1+z_L} \frac{D_{LS}}{D_L} v_O, \quad (1)$$

where D refers to the angular diameter distance, and the subscripts ‘ O ’, ‘ L ’, and ‘ S ’ refer to the *Observer*, *Lens* and *Source* planes, respectively. This velocity v' is the velocity the GW source ‘appears’ to have in the source plane, relative to a frame where the observer and lens are not moving. This also illustrates that the GW phase shift we observe and here consider generally reflects information about the *combined* cosmologically weighted relative velocities between observer, lens, and source. However, it is possible to subtract the

observer velocity, and if the lens is a massive galaxy cluster, then it can be argued that the velocity of the GW source dominates.

For deriving the GW phase shift induced by the relative velocity v' , we now consider a strongly lensed GW source with two observed GW images, or GW signals, that after observation have been aligned such that their time of merger coincides (shifted by the time-delay, Δt). If the GW source has a non-zero velocity relative to the lens and observer, i.e. if $v' > 0$ from Eq. 1, then the two images will show a time-dependent temporal displacement from the point-of-merger (see Fig. 1). If we denote this time displacement τ , then the corresponding displacement in terms of orbital cycles in units of radians, referred to as the *GW phase shift*, can be expressed as,

$$\delta\phi = 2\pi\tau/T, \quad (2)$$

where T is the orbital time of the binary GW source (e.g. Samsing et al. 2024a; Hendriks et al. 2024a,b). Note here that $2/T$ is the GW frequency in the case of circular GW sources; however, this is not the case of eccentric GW sources, as they emit with a much broader spectrum. The GW signal will however still be period with time T , which is why we use this timescale in this general formulation of GW phase shift (see also Samsing et al. (2024a)).

In our considered lensing case, the time τ is what encodes all the information about the lens setup and relative motion, and can be estimated by considering the variation in the time-delay surface as the GW source is moving. The kinematics of the movement relates to a change in the angular position of the GW source, $\Delta\beta$, as follows (see Fig. 1),

$$\Delta\beta = \frac{1}{1+z_S} \frac{v't}{D_S}, \quad (3)$$

where t is defined in the observer frame, which then can be translated into τ as (Samsing et al. 2024a),

$$\tau \approx 2\theta \frac{D_L}{D_{LS}} \frac{1+z_L}{1+z_S} \frac{v'}{c} t, \quad (4)$$

where 2θ equals the angular separation between the two images, and c is the speed of light. Substituting this into Eq. 2, one now finds the general form for $\delta\phi$,

$$\delta\phi = 4\pi\theta \frac{v_d}{c} \frac{t}{T(t)}, \quad (5)$$

where the velocity v_d ,

$$v_d = v_O + \frac{D_L}{D_{LS}} \frac{1+z_L}{1+z_S} v_S - \frac{D_S}{D_{LS}} v_L, \quad (6)$$

represents an ‘effective Doppler velocity’.

In relation to the actual astrophysical observables, the GW phase shift in Eq. 5 is the key observable, but to constrain

the value of v_d one must also have an estimate for at least θ . In electromagnetic observations of strong gravitational lensing, θ is relatively easy to measure, but the extremely poor sky localization for GWs makes it near impossible for lensed GW sources. However, if a lens model is assumed, θ can be inferred from other observables, namely the ratio between image magnifications and the time-delay between the lensed images (e.g. Itoh et al. 2009). For example, for a Singular Isothermal Sphere (SIS) lens, the ratio between the magnification factors of the two observed images, $F_{12} = \mu_1/\mu_2 > 1$ can be written as,

$$F_{12} = \frac{\mu_1}{\mu_2} \approx \frac{\theta_E + \beta}{\theta_E - \beta}, \quad (7)$$

where θ_E is the Einstein angle (note that with our notation $2\theta_E \approx 2\theta$), and β is the angular position of the GW source. The corresponding time difference between the two images, Δt , is given by

$$\Delta t \approx \frac{2D_L D_S}{D_{LS}} \frac{1+z_L}{c} \beta \theta_E. \quad (8)$$

By combining Eq. 7 and Eq. 8, one can now isolate for θ_E ,

$$\theta_E = \left(\frac{D_{LS}}{D_L D_S} \frac{c \Delta t}{2(1+z_L)} \frac{F_{12} + 1}{F_{12} - 1} \right)^{1/2}, \quad (9)$$

which then can be used in Eq. 5 to approximate θ . For a better estimate one naturally has to employ a more sophisticated model for the lens (e.g. Vujeva et al. 2025) and an estimator for the angular diameter distances; however, this is beyond this work, and we therefore proceed with θ as our variable to keep our analysis more general.

2.2. General Relations

Assuming that v_d , and our lensing setup remain constant over the duration of observation, t , it is clear from Eq. 5 that the evolution of the GW phase shift is dictated by how T relates to t . As we are considering binary systems in this work, the time T can be written as,

$$T(t) = 2\pi \sqrt{\frac{a(t)^3}{2Gm}}, \quad (10)$$

where m is the mass of binary’s components ($m_1 = m_2 = m$), $a(t)$ is the semi-major axis (SMA) of the binary at time t . If we assume that $a(t) \propto t^\alpha$, then the GW phase shift will follow the general scaling,

$$\delta\phi \propto t^{1-3\alpha/2} \quad (a \propto t^\alpha). \quad (11)$$

By now defining the critical value for α , $\alpha_c = 2/3$, then for $\alpha > \alpha_c$ the GW phase shift $\delta\phi$ will *decrease* with time, whereas if $\alpha < \alpha_c$ then $\delta\phi$ will *increase*. For example, for circular GW sources driven by GW radiation, $\alpha = 1/4$ (e.g.

Peters 1964), which leads to $\delta\phi \propto t^{5/8}$. Depending on the (combination) of dissipative mechanisms for our considered lensed inspiraling binary system, e.g. effects from gas or other external forces (e.g. Barausse et al. 2014; Zwick et al. 2023; Samsing et al. 2024a), the evolution of the GW phase shift will show different characteristics. Below we will study properties of eccentric evolving GW sources from formation to merger.

3. ECCENTRIC GRAVITATIONAL WAVE SOURCES

In the following we derive and study the evolution of the GW phase shift induced by the relative transverse motion v_d , defined to Eq. 5 and Eq. 6, for an eccentric GW source, as a function of time, eccentricity and GW frequency. In all our derivations we assume for simplicity that each of the binary objects have equal and constant mass m , from which it follows from Eq. 5 and Eq. 10 that,

$$\delta\phi = \sqrt{8G} \times \theta \frac{v_d}{c} m^{1/2} \frac{t}{a(t)^{3/2}}. \quad (12)$$

The exercise therefore becomes to relate $a(t)$ and t to the properties of the eccentric GW source, as we illustrate in the following. In all our calculations we assume Peters (1964) relations for the evolution of the orbital elements, with a note on the limits of this formalism (e.g. Zwick et al. 2020). For a more accurate calculation, one can e.g. use full GW forms and simply shift them by τ using Eq. 4.

For the examples shown in the following we also refer to our *Fiducial Model*, for which we assume the following values for illustrative purposes; $v_d = 1500 \text{ km/s}$, $m = 5M_\odot$, $\theta = 25''$ (25 arcsec), and an initial GW peak frequency (see below) at formation of $f_0 = 2 \text{ Hz}$ assuming GW capture from a parabolic orbit (see also Samsing et al. (2024a))

3.1. Evolution with Time

We start by considering the GW phase shift as a function of time t , defined in the observer frame. It is unfortunately not possible to algebraically isolate $\delta\phi$ as a function of t using Peters (1964) for the general eccentric case, but insight can be gained from considering the two limits for which the binary eccentricity approaches $e = 0$ (near merger) and $e = 1$ (near initial assembly). We do that in the following.

In the $e = 0$ limit, the time t relates to the binary parameters as (Peters 1964),

$$t_c = \frac{5}{512} \frac{c^5}{G^3} \frac{a^4}{m^3}, \quad (e = 0). \quad (13)$$

Now inserting this into the above Eq. 12, one finds the GW phase shift to evolve as,

$$\delta\phi = \sqrt{8} \left(\frac{5}{512} \right)^{3/8} \left(\frac{c^3}{G} \right)^{5/8} \theta \frac{v_d}{c} \frac{t^{5/8}}{m^{5/8}}, \quad (e = 0) \quad (14)$$

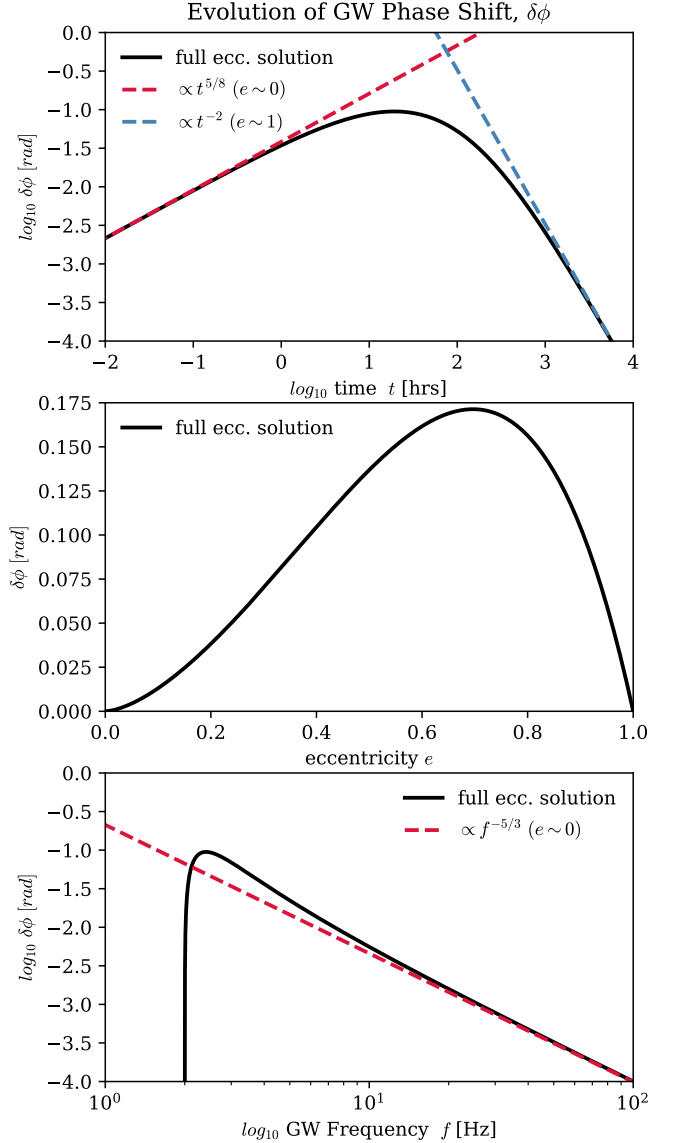


Figure 2. Evolution of Gravitational Wave Phase Shift: The figure shows the GW phase shift, $\delta\phi$, as a function of time, t , eccentricity, e , and GW frequency, f , for our illustrative *Fiducial Model* outlined in Sec. 3 ($v_d = 1500 \text{ km/s}$, $m = 5M_\odot$, $\theta = 25''$). Note here that $\delta\phi \propto \theta v_d$ in all our cases. *Top plot:* Here is shown $\log\delta\phi, \log t$ when going backwards from merger ($e \sim 0$) towards assembly ($e \sim 1$). The two asymptotic limits, $\delta\phi \propto t^{5/8}$ ($e \sim 0$) and $\delta\phi \propto t^{-2}$ ($e \sim 1$), are shown with *dashed lines*, where the *solid black line* is the result of solving Peters (1964) equations in combination with Eq. 12. Note how the circular limit keeps growing, where the eccentric turns around. *Middle plot:* Evolution of $\delta\phi$ as a function of GW source eccentricity, e , given by Eq. 19. This suggests that the maximum GW phase shift will occur at $e \sim 0.7$. *Bottom plot:* plot of $\log\delta\phi$ as a function of $\log f$, where the *solid black line* is derived using Peters (1964) (note the approximate solution given by Eq. 26), and the *red dashed line* shows the circular asymptotic limit, $\delta\phi \propto f^{-5/3}$. Results are discussed in Sec. 3.

which also was worked out in [Samsing et al. \(2024b\)](#). We now extend this to the eccentric limit, where the time t instead relates to $a(t)$ as ([Peters 1964](#)),

$$t_e \approx t_c \times (1 - e^2)^{7/2}, \quad (e > 0). \quad (15)$$

Note here that we have omitted the front factor (768/425) to ensure our scalings naturally asymptote the circular limit when the GW source approaches merger. As the binary peri-center distance, r_p , remains nearly constant in the eccentric limit, the merger time will here instead scale as $t_e \propto r_p^{7/2} a(t)^{1/2} \propto a(t)^{1/2}$, where we have used $r_p = a(1 - e)$. This instead leads to the following relation,

$$\delta\phi \propto \theta \frac{v_d}{c} \frac{t^{-2}}{m^{5/8}}, \quad (e \sim 1). \quad (16)$$

When going backwards in time from the point of merger, the GW phase shift therefore first increases $\propto t^{5/8}$, until $\delta\phi$ reaches a maximum, after which it decreases $\propto t^{-2}$. These two scalings, together with a curve derived by numerically evolving [Peters \(1964\)](#) coupled differential equations for da/dt and de/dt , are shown in the top plot of [Fig. 2](#) for our *Fiducial Model* parameters. The largest difference is clearly seen at earlier times, as the eccentric case decreases in contrast to the circular. This essentially implies that steadily accumulating GW phase shift when going backwards in time from merger is not always possible in the eccentric case, in contrast to the circular. We explore this further below.

3.2. Evolution with Eccentricity

The evolution of $\delta\phi$ can be written out analytically as a function of binary eccentricity, e , which allows one to study properties such as maximum GW phase shift and eventually dependence on GW frequency. For this we start by using the relation between a and e as given by ([Peters 1964](#)),

$$a(e) \approx \frac{2r_0 e^{12/19}}{(1 - e^2)} \frac{g(e)}{g(1)}, \quad (e_0 \approx 1), \quad (17)$$

where

$$g(e) = \left(1 + 121e^2/304\right)^{870/2299}, \quad (18)$$

and we have assumed that the initial eccentricity $e_0 \approx 1$, and defined the initial peri-center distance $r_0 = a_0(1 - e_0)$ (e.g. [Samsing et al. 2024a](#)). By now using this relation together with [Eq. 12](#) and [Eq. 15](#), we find that $\delta\phi$ can be expressed as a function of eccentricity as,

$$\delta\phi = \frac{2^{5/2}\sqrt{8}}{g(1)^{5/2}} \frac{5}{512} \frac{c^5}{G^{5/2}} \times \theta \frac{v_d}{c} \frac{r_0^{5/2}}{m^{5/2}} \times F(e), \quad (19)$$

where the evolution is entirely encoded in the function,

$$F(e) = e^{30/19} (1 - e^2) g(e)^{5/2}. \quad (20)$$

The maximum GW phase shift will therefore occur where $F(e)$ has its maximum, which is where the eccentricity e equals,

$$e_m = \sqrt{\frac{\sqrt{107329}}{331} - \frac{167}{331}} \approx 0.7. \quad (21)$$

This is a moderate value, e.g. in the case of GW phase shift from accelerated sources $e_m \sim 0.95$ ([Samsing et al. 2024a](#)), and should therefore be observable in the near future with the ongoing effort in modeling accurate eccentric GW forms. The middle plot of [Fig. 2](#) shows $F(e)$ as a function of e .

3.3. Evolution with Frequency

GW frequency for eccentric GW sources and how it relates to eccentricity and observables, is a matter of definition (e.g. [Vijaykumar et al. 2024](#)). Here we work with the GW frequency where most of the GW power is radiated over one orbit, which is often referred to as the *GW peak frequency*, f . This can be approximated by,

$$f \approx \frac{1}{\pi} \sqrt{\frac{2Gm}{r_p^3}}, \quad (22)$$

where r_p is the orbital peri-center distance. Note here that as r_p stays approximately constant during inspiral, so will the GW peak frequency, until the binary has circularized and starts decaying as a standard circular source with $f \propto t^{-3/8}$. With the above relation for f , we can now rewrite [Eq. 19](#) from above in the following forms,

$$\begin{aligned} \delta\phi &= \frac{2^{10/3}\sqrt{8}}{g(1)^{5/2}\pi^{5/3}} \frac{5}{512} \frac{c^5}{G^{5/3}} \times \theta \frac{v_d}{c} m^{-5/3} f_0^{-5/3} \times F(e), \\ &= \frac{2^{5/6}\sqrt{8}}{\pi^{5/3}} \frac{5}{512} \frac{c^5}{G^{5/3}} \times \theta \frac{v_d}{c} m^{-5/3} f^{-5/3} \times H(e), \\ &= \delta\phi(e=0) \times H(e), \end{aligned} \quad (23)$$

where

$$H(e) = (1 + e)^{7/2} (1 - e). \quad (24)$$

In the last equality of [Eq. 23](#), we have expressed the evolution in terms of the circular limit $\delta\phi(e=0)$, which naturally is the asymptotic solution for $e \rightarrow 0$. From the above relations it follows that $H(e)$ describes how much the eccentric case deviates from the circular limit. For example, the maximum value of $\delta\phi$ relative to $\delta\phi(e=0)$ at a given GW frequency will be the maximum of $H(e)$,

$$\max \left[\frac{\delta\phi}{\delta\phi(e=0)} \right] = \frac{10976\sqrt{14}}{19683} \approx 2, \quad (e = \frac{5}{9} \approx 0.6), \quad (25)$$

with corresponding value for e shown in the parenthesis. The function $H(e)$ is shown in [Fig. 3](#) as a function of e . That the expected maximum increase in $\delta\phi$ is ~ 2 is not significant compared to e.g. a factor of ~ 30 for accelerated sources

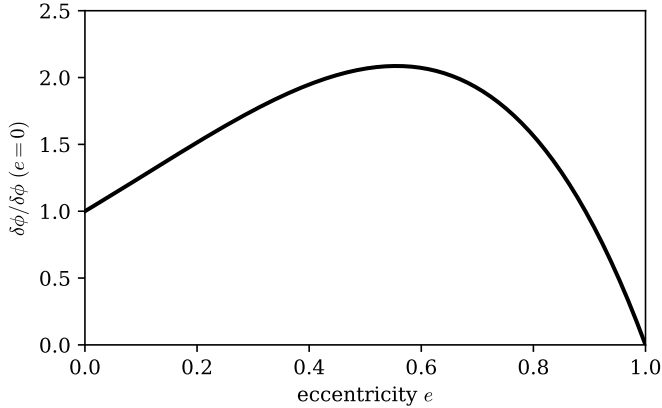


Figure 3. Eccentric GW Source Relative to Circular: The figure shows the function $H(e)$ defined in Eq. 23 and Eq. 24, which equals the ratio in GW phase shift between the eccentric case and the circular case, $\delta\phi/\delta\phi(e=0)$, evaluated at the same GW frequency f (note here that f in the eccentric case refers to the GW peak frequency defined in Eq. 22). As seen, when going backwards in time from merger ($e \sim 0$), the ratio steadily rises until it reaches a maximum $\delta\phi/\delta\phi(e=0) \sim 2$ at $e \sim 0.6$, after which it decreases towards 0 when $e \rightarrow 1$, or equivalently at $f = f_0$. The eccentric and circular cases can be seen separately in Fig. 2.

(Samsing et al. 2024a), but does illustrate that the eccentric limit at least is not suppressing the GW phase shift, and should further have a unique shape that is observable.

For analytically being able to study how $\delta\phi$ evolves as a function of f in our considered eccentric case, we make the following approximation, $(f/f_0)^{-2/3} \approx e^{12/19}$, that leads to $e \approx (f_0/f)^{19/18} \approx (f_0/f)$, which follows from Eq. 17 and valid in the high eccentricity limit (e.g. Samsing et al. 2024a). Substituting this into Eq. 23 it now follows that,

$$\delta\phi(f) \approx \delta\phi(f, e=0) \times (1 + f_0/f)^{7/2} (1 - f_0/f). \quad (26)$$

This relation with the circular asymptotic limit is shown in the bottom plot of Fig. 2 for our *Fiducial Model* parameters. As seen, the eccentric limit rises above the circular limit as the eccentricity increases towards lower f , as described by $H(e)$. When the eccentricity reaches the value e_m given by Eq. 21, the GW phase shift rapidly starts decreasing for then to reach zero at $e \sim 1$, or equivalently when $f = f_0$. Depending on the GW detector, only parts of this evolution might be observable, e.g. ET and CE would likely be able to observe most of the shown evolution, whereas LIGO will see the signal only when $f > 10$ Hz at which the GW source has almost reached its circular asymptotic limit and with a greatly reduced $\delta\phi$.

The GW frequency at which the maximum $\delta\phi$ is reached can be found by rewriting Eq. 17 in terms of f , such that

$$\frac{f}{f_0} \approx \left(\frac{(1+e)g(1)}{2e^{12/19}g(e)} \right)^{3/2}, \quad (27)$$

$$\approx 1.2, \quad (e = e_m).$$

As seen, the GW frequency at $\max(\delta\phi)$ is only higher by a factor of ~ 1.2 compared to the GW frequency at formation, f_0 , which tells that to observe the GW source near its maximum $\delta\phi$, the detector also have to operate down to frequencies $\sim f_0$. For GW sources formed through dynamics, a significant fraction will distribute with f_0 between $1 - 10$ Hz (e.g. Zevin et al. 2019; Samsing et al. 2020), and a significant part of the evolution of $\delta\phi$, especially near its maximum, is therefore expected to be observed in the coming years.

4. CONCLUSIONS

The (relative transverse) proper motion can normally not be measured for GW sources, but it is possible to constrain for strongly lensed GW sources, as the different images allow the observer to see the GW source from different LOS. This is done by comparing the GW phase evolution between images, or lensed GW signals, from which one can infer a relative GW shift that can be mapped to the motion of the GW source.

In this paper, we explored for the first time the expected evolution of this GW phase shift for a simple two-image lens model, as a function of time, binary eccentricity, and GW peak frequency. We especially find that the GW phase shift evolution as a function of eccentricity, e , takes a unique form $\propto e^{30/10}(1-e^2)g(e)^{5/2}$ (Eq. 20), that only depends on eccentricity, from which we derived that the maximum GW phase shift occurs at $e \sim 0.7$ with an enhancement of ~ 2 compared to the circular case.

A significant fraction of the expected GW mergers and lensed GW sources that we will observe in the coming decades with LIGO, ET and CE (e.g. Xu et al. 2022; Smith et al. 2023), will be eccentric (e.g. Samsing 2018; Rodriguez et al. 2018). Our present study clearly suggests that the GW phase shift should be possible to observe also for this population (for SNR calculations in the circular case see Samsing et al. (2024b)), which opens up immense possibilities, and the natural question if the eccentric GW population (dominated by the dynamical channel) is expected to have a different distribution in relative proper motion across redshift compared to the more generic circular GW population (dominated likely by the isolated binary evolution channel). In other words, can our suggested measure of relative velocity be used for probing the nature and origin of GW sources? In upcoming papers we will explore these questions both in relation to GW populations and assembly theory, as well as the possible impact that a measure of transverse velocity for hundreds of lensed GW sources could have on cosmology.

5. ACKNOWLEDGMENTS

The authors are grateful Juan Urrutia, Mikołaj Korzyński, Miguel Zumalacárregui, and Graham Smith, for useful discussions. We further thank the The Erwin Schrödinger International Institute for Mathematics and Physics (ESI) and

the organizers of the workshop "Lensing and Wave Optics in Strong Gravity" where part of this work was carried out. K.H, L.Z., P.S., and J.S. are supported by the Villum Fonden grant No. 29466, and by the ERC Starting Grant no. 101043143

– BlackHoleMergs led by J. Samsing. R.L and L.V. are supported by the research grant no. VIL37766 and no. VIL53101 from Villum Fonden, and the DNRF Chair program grant no. DNRF162 by the Danish National Research Foundation.

REFERENCES

- Barausse, E., Cardoso, V., & Pani, P. 2014, *PhRvD*, 89, 104059, doi: [10.1103/PhysRevD.89.104059](https://doi.org/10.1103/PhysRevD.89.104059)
- Birkinshaw, M. 1989, in *Gravitational Lenses*, ed. J. M. Moran, J. N. Hewitt, & K.-Y. Lo, Vol. 330, 59, doi: [10.1007/3-540-51061-3_36](https://doi.org/10.1007/3-540-51061-3_36)
- Chitre, S. M., & Saslaw, W. C. 1989, *Nature*, 341, 38, doi: [10.1038/341038a0](https://doi.org/10.1038/341038a0)
- D’Orazio, D. J., & Loeb, A. 2020, *PhRvD*, 101, 083031, doi: [10.1103/PhysRevD.101.083031](https://doi.org/10.1103/PhysRevD.101.083031)
- Fabj, G., & Samsing, J. 2024, arXiv e-prints, arXiv:2402.16948. <https://arxiv.org/pdf/2402.16948>
- Gondán, L., & Kocsis, B. 2022, *MNRAS*, 515, 3299, doi: [10.1093/mnras/stac1985](https://doi.org/10.1093/mnras/stac1985)
- Gültekin, K., Miller, M. C., & Hamilton, D. P. 2006, *ApJ*, 640, 156
- Hendriks, K., Zwick, L., & Samsing, J. 2024a, arXiv e-prints, arXiv:2408.04603, doi: [10.48550/arXiv.2408.04603](https://doi.org/10.48550/arXiv.2408.04603)
- Hendriks, K., Atallah, D., Martinez, M., et al. 2024b, arXiv e-prints, arXiv:2411.08572, doi: [10.48550/arXiv.2411.08572](https://doi.org/10.48550/arXiv.2411.08572)
- Hu, W.-R., & Wu, Y.-L. 2017, *National Science Review*, 4, 685, doi: [10.1093/nsr/nwx116](https://doi.org/10.1093/nsr/nwx116)
- Itoh, Y., Futamase, T., & Hattori, M. 2009, *PhRvD*, 80, 044009, doi: [10.1103/PhysRevD.80.044009](https://doi.org/10.1103/PhysRevD.80.044009)
- Kawamura, S., Ando, M., Seto, N., et al. 2011, *Classical and Quantum Gravity*, 28, 094011, doi: [10.1088/0264-9381/28/9/094011](https://doi.org/10.1088/0264-9381/28/9/094011)
- Kayser, R., Refsdal, S., & Stabell, R. 1986, *A&A*, 166, 36
- Liu, B., Lai, D., & Wang, Y.-H. 2019, *ApJ*, 881, 41, doi: [10.3847/1538-4357/ab2dfb](https://doi.org/10.3847/1538-4357/ab2dfb)
- Liu, S., Hu, Y.-M., Zhang, J.-d., & Mei, J. 2020, *PhRvD*, 101, 103027, doi: [10.1103/PhysRevD.101.103027](https://doi.org/10.1103/PhysRevD.101.103027)
- Luo, J., Chen, L.-S., Duan, H.-Z., et al. 2016, *Classical and Quantum Gravity*, 33, 035010, doi: [10.1088/0264-9381/33/3/035010](https://doi.org/10.1088/0264-9381/33/3/035010)
- Peters, P. C. 1964, *Physical Review*, 136, 1224, doi: [10.1103/PhysRev.136.B1224](https://doi.org/10.1103/PhysRev.136.B1224)
- Rodriguez, C. L., Amaro-Seoane, P., Chatterjee, S., et al. 2018, *PhRvD*, 98, 123005, doi: [10.1103/PhysRevD.98.123005](https://doi.org/10.1103/PhysRevD.98.123005)
- Samsing, J. 2018, *PhRvD*, 97, 103014, doi: [10.1103/PhysRevD.97.103014](https://doi.org/10.1103/PhysRevD.97.103014)
- Samsing, J., Askar, A., & Giersz, M. 2018a, *ApJ*, 855, 124, doi: [10.3847/1538-4357/aab52](https://doi.org/10.3847/1538-4357/aab52)
- Samsing, J., & D’Orazio, D. J. 2018, *MNRAS*, doi: [10.1093/mnras/sty2334](https://doi.org/10.1093/mnras/sty2334)
- Samsing, J., D’Orazio, D. J., Kremer, K., Rodriguez, C. L., & Askar, A. 2020, *PhRvD*, 101, 123010, doi: [10.1103/PhysRevD.101.123010](https://doi.org/10.1103/PhysRevD.101.123010)
- Samsing, J., Hamers, A. S., & Tyles, J. G. 2019, *PhRvD*, 100, 043010, doi: [10.1103/PhysRevD.100.043010](https://doi.org/10.1103/PhysRevD.100.043010)
- Samsing, J., Hendriks, K., Zwick, L., D’Orazio, D. J., & Liu, B. 2024a, arXiv e-prints, arXiv:2403.05625, doi: [10.48550/arXiv.2403.05625](https://doi.org/10.48550/arXiv.2403.05625)
- Samsing, J., & Ilan, T. 2018, *MNRAS*, 476, 1548, doi: [10.1093/mnras/sty197](https://doi.org/10.1093/mnras/sty197)
- Samsing, J., MacLeod, M., & Ramirez-Ruiz, E. 2014, *ApJ*, 784, 71, doi: [10.1088/0004-637X/784/1/71](https://doi.org/10.1088/0004-637X/784/1/71)
- . 2018b, *ApJ*, 853, 140, doi: [10.3847/1538-4357/aaa715](https://doi.org/10.3847/1538-4357/aaa715)
- Samsing, J., & Ramirez-Ruiz, E. 2017, *ApJL*, 840, L14, doi: [10.3847/2041-8213/aa6f0b](https://doi.org/10.3847/2041-8213/aa6f0b)
- Samsing, J., Bartos, I., D’Orazio, D. J., et al. 2022, *Nature*, 603, 237, doi: [10.1038/s41586-021-04333-1](https://doi.org/10.1038/s41586-021-04333-1)
- Samsing, J., Zwick, L., Saini, P., et al. 2024b, arXiv e-prints, arXiv:2412.14159, doi: [10.48550/arXiv.2412.14159](https://doi.org/10.48550/arXiv.2412.14159)
- Savastano, S., Vernizzi, F., & Zumalacárregui, M. 2024, *PhRvD*, 109, 024064, doi: [10.1103/PhysRevD.109.024064](https://doi.org/10.1103/PhysRevD.109.024064)
- Smith, G. P., Robertson, A., Mahler, G., et al. 2023, *MNRAS*, 520, 702, doi: [10.1093/mnras/stad140](https://doi.org/10.1093/mnras/stad140)
- Vijaykumar, A., Hanselman, A. G., & Zevin, M. 2024, *ApJ*, 969, 132, doi: [10.3847/1538-4357/ad4455](https://doi.org/10.3847/1538-4357/ad4455)
- Vujeva, L., María Ezquiaga, J., Lo, R. K. L., & Chan, J. C. L. 2025, arXiv e-prints, arXiv:2501.02096, doi: [10.48550/arXiv.2501.02096](https://doi.org/10.48550/arXiv.2501.02096)
- Wucknitz, O., & Sperhake, U. 2004, *PhRvD*, 69, 063001, doi: [10.1103/PhysRevD.69.063001](https://doi.org/10.1103/PhysRevD.69.063001)
- Xu, F., Ezquiaga, J. M., & Holz, D. E. 2022, *ApJ*, 929, 9, doi: [10.3847/1538-4357/ac58f8](https://doi.org/10.3847/1538-4357/ac58f8)
- Yang, X.-Y., Chen, T., & Cai, R.-G. 2024, arXiv e-prints, arXiv:2410.16378, doi: [10.48550/arXiv.2410.16378](https://doi.org/10.48550/arXiv.2410.16378)
- Zevin, M., Romero-Shaw, I. M., Kremer, K., Thrane, E., & Lasky, P. D. 2021, *ApJL*, 921, L43, doi: [10.3847/2041-8213/ac32dc](https://doi.org/10.3847/2041-8213/ac32dc)
- Zevin, M., Samsing, J., Rodriguez, C., Haster, C.-J., & Ramirez-Ruiz, E. 2019, *ApJ*, 871, 91, doi: [10.3847/1538-4357/aaf6ec](https://doi.org/10.3847/1538-4357/aaf6ec)
- Zwick, L., Capelo, P. R., Bortolas, E., Mayer, L., & Amaro-Seoane, P. 2020, *MNRAS*, 495, 2321, doi: [10.1093/mnras/staa1314](https://doi.org/10.1093/mnras/staa1314)
- Zwick, L., Capelo, P. R., & Mayer, L. 2023, *MNRAS*, 521, 4645, doi: [10.1093/mnras/stad707](https://doi.org/10.1093/mnras/stad707)